How particle collisions increase the rate of accretion from the cosmological background onto primordial black holes in braneworld cosmology

V. V. Tikhomirov [*] and Y. A. Tsalkou [†]

Institute for Nuclear Problems, Belarussian State University, Bobruiskaya 11, 220050 Minsk, Belarus

(Dated: February 5, 2008)

It is shown that, contrary to the widespread opinion, particle collisions considerably increase accretion rate from the cosmological background onto 5D primordial black holes formed during the high-energy phase of the Randall-Sundrum Type II braneworld scenario. Increase of accretion rate leads to much tighter constraints on initial primordial black hole mass fraction imposed by the critical density limit and measurements of high-energy diffuse photon background and antiproton excess.

It is well known that primordial black holes (PBHs) open up a way to obtain information on earliest era of the Universe [1, 2]. Recent works [3, 4, 5, 6, 7, 8] show that PBHs can also be a probe of braneworld cosmologies. The Hawking temperature drop [3] and considerable PBH mass growth due to radiation dominated background accretion occur [4] in the simplest braneworld cosmology of the Randall-Sundrum Type II (RS2). These modifications of PBH properties provide new constraints on the initial PBH mass fraction [6, 7, 8]. PBH mass growth is exponentially sensitive to the accretion efficiency. However, authors of [6, 7, 8] considered the accretion efficiency as a free parameter. In fact, they started with F equals 1 in the case of collisionless radiative background and assumed that it can only *decrease* when relativistic particle scattering length is small. They also predicted that a sufficiently low value of F leads to weaker constraints than those obtained in the standard 4D cosmology. It also allow the restriction of the RS2 curvature radius l from below. Meanwhile, according to the theory of spherical accretion of nonrelativistic particles [9], the hydrodynamic accretion theory [10] should be used instead of collisionless accretion theory [11, 12] for small scattering length. Since *"the presence of collisions between particles restricts tangential motion and funnels particles effectively in the radial direction for efficient capture"* [9], the hydrodynamic accretion rate substantially exceeds the collisionless one in the case of nonrelativistic particles. The aim of the present paper is to demonstrate that collisions of relativistic particles analogously *increase* the accretion rate of the radiation dominated background and lead to the new, much tighter, constraints.

Let us remind the reader that in the RS2 model our Universe is a 4D Lorentz metric hypersurface called a *brane*, embedded in a Z_2 symmetric 5D anti-de Sitter spacetime called the *bulk*, characterized by the curvature radius l, presently bound [13] by condition $l \leq 0.2mm$. A black hole (BH) behaves as an essentially 5D object described by the metric [3, 4, 5, 6, 7, 8]

$$ds^2 = -\left(1 - r_{BH}^2/r^2\right) dt^2 + \frac{1}{(1 - r_{BH}^2/r^2)} dr^2 + r^2 d\Omega_2^2,$$

(1)

where $d\Omega_2^2$ is the line element on a unit 2-sphere, if its modified Schwarzschild radius

$$r_{BH} = \sqrt{\frac{8}{3\pi}} \sqrt{\frac{l}{l_4}} \sqrt{\frac{M}{M_4}} l_4$$

(2)

is much smaller than l. We use the units where $c = G = 1$ and introduce 4D Planck scale quantities l_4, M_4 and t_4 for convenience. The high energy brane regime is characterized [3] by scale factor, energy density, horizon mass, and duration

$$a = a_h \left(\frac{t}{t_h}\right)^{1/2}, \qquad \rho = \frac{3}{32\pi} \frac{M_4^2}{t_c\, t},$$
$$M_h = 8M_4^2 \frac{t^2}{t_c}, \qquad t_c = t_4 \frac{l}{2l_4},$$

(3)

where t is cosmic time, and $t_h < t_c$. It is usually assumed [1, 2, 3, 4, 5, 6, 7, 8] that at formation time t_i the PBH mass is

$$M_i = fM_h(t_i).$$

(4)

The condition $r_{BH} \ll l$ is fulfilled if $f \sim 1$ and $t_i < t_c$.

The accretion rate

$$\frac{dM}{dt} = F4\pi r_{BH}^2 \, \rho(t)$$

(5)

and energy density (3) lead to exponential BH mass growth

$$M(t) = M_i \left(\frac{t}{t_i}\right)^{2F/\pi}$$

(6)

at $t < t_c$ [4]. In fact, Eq. (5) is justified [5] only in the case of collisionless relativistic particles when accretion

---

efficiency F equals 1. However, a simple comparison of the scattering length l_{sc} with the radius (2) demonstrates that the cosmological background cannot be considered as a collisionless particle medium in the case of PBH masses most relevant for observational constraints. In fact, the opposite condition $l_{sc} \ll r_{BH}$ is true, in general, for such PBHs. It allows one to treat the accreting cosmological background as a continuous medium. Therefore, to obtain F one should evaluate the accretion rate (5) in hydrodynamic approximation.

Since radiation dominated background is characterized by an indefinite particle number, the momentum conservation equation

$$(\rho + P)u_{i;k}u^k = -P_{,i} - u_i P_{,k} u^k, \qquad (7)$$

should be used [14] together with the entropy conservation equation

$$(\sigma u^k)_{;k} = 0. \qquad (8)$$

Here comma and semicolon denote usual and covariant derivatives; ρ, σ, P and u^i are energy and entropy densities, pressure and 4-velocity of accretion flow, respectively. In the metric (1) adiabatic accretion equations (7) and (8) take the form

$$uu' + \frac{r_{BH}^2}{r^3} + \frac{P'}{\rho + P}\left(1 + u^2 - \frac{r_{BH}^2}{r^2}\right) = 0 \qquad (9)$$

and

$$\frac{\sigma'}{\sigma} + \frac{u'}{u} + \frac{2}{r} = 0 \qquad (10)$$

where $u = u^1$ is the radial component of 4-velocity and primes denote the derivative with respect to r. The radiation dominated background is described by equations [15]

$$\rho(T) = 3P(T) = \frac{\pi^2}{30}g_{eff}T^4 \qquad (11)$$

and

$$\sigma(T) = \frac{2\pi^2}{45}g_{eff}T^3, \qquad (12)$$

where g_{eff} is the number of relativistic particle species at temperature T. The value $g_{eff} \simeq 100$ will be used below because $T \geq 1 TeV$ at $t < t_c$. Equations (11) and (12) allow to rewrite Eqs. (9) and (10) in terms of temperature

$$uu' + \frac{r_{BH}^2}{r^3} + \frac{T'}{T}\left(1 + u^2 - \frac{r_{BH}^2}{r^2}\right) = 0, \qquad (13)$$

$$3\frac{T'}{T} + \frac{u'}{u} + \frac{2}{r} = 0. \qquad (14)$$

Solving Eq. (13) and (14) for u' and T', one obtains (compare with [9])

$$u' = \frac{D_1}{D}, \qquad T' = -\frac{D_2}{D}, \qquad (15)$$

where

$$D = \frac{2u^2 - 1 + r_{BH}^2/r^2}{uT}, \qquad (16)$$

$$D_1 = \frac{2u^2 + 2 - 5r_{BH}^2/r^2}{rT} \qquad (17)$$

and

$$D_2 = \frac{2u^2 - r_{BH}^2/r^2}{ru}. \qquad (18)$$

To avoid singularities in the accretion flow, the solution of Eqs. (15) must pass through a "critical" or "sound" point $r = r_s$ where $D = D_1 = D_2 = 0$. Solving equations $D = D_1 = D_2 = 0$, one obtains

$$r_s = \sqrt{2}\, r_{BH} \qquad (19)$$

and

$$u_s = u(r_s) = \frac{1}{2} \qquad (20)$$

in light speed units.

Integration of Eq. (13) leads to a conservation law

$$\left(1 + u^2 - \frac{r_{BH}^2}{r^2}\right)T^2 = const = T_b^2; \qquad (21)$$

where T_b is the background temperature defined by expressions (3) and (11) for energy density [3]. Substituting Eqs. (19) and (20) into Eq. (21) one obtains

$$T_s = T(r_s) = \frac{2}{\sqrt{3}}T_b. \qquad (22)$$

Direct integration of Eq. (10) shows that the term $r^2\sigma(r)u(r)$ does not depend on r, while Eqs. (19), (20) and (22) allow to evaluate its value

$$r^2\sigma(r)u(r) = r_s^2\sigma(r_s)u(r_s). \qquad (23)$$

Applying the latter equation sufficiently far from BH, where $T(r) \to T_b$, and using Eqs. (12), (19), (20), and (22), one obtains

$$u(r) \simeq \frac{8}{3\sqrt{3}} \times \frac{r_{BH}^2}{r^2}, \qquad r \gg r_{BH}. \qquad (24)$$

Substituting $r \gg r_{BH}$, $T(r) \simeq T_b$, $\rho(r) \simeq \rho(T_b) \equiv \rho(t)$ and Eq. (24) into the formula

$$\frac{dM}{dt} = 4\pi r^2 \rho(r)u(r) \qquad (25)$$

we finally come to the accretion rate (5) with the accretion efficiency

$$F = \frac{8}{3\sqrt{3}} \simeq 1.54 \qquad (26)$$

describing radiation dominated background accretion in hydrodynamic approximation applicable in the limit of frequent particle collisions. Since (26) exceeds 1, particle collisions, in fact, increase both accretion rate (5) and PBH mass growth coefficient (6).

Let us now demonstrate that continuous approximation is indeed valid for the most of the high-energy phase. Since the characteristic space scale (19) of accretion flow is determined by r_{BH}, one should compare r_{BH} with the scattering length $l_{sc} = l_{sc}(t) \simeq 1/\sigma n$. Here $n = n(T_b) \sim \rho(T_b)/3T_b$ is the particle number density and $\sigma = \sigma(T_b) \simeq \alpha^2/T_b^2$ is the scattering cross section in which $\alpha = \alpha(T_b)$ is the interaction constant.

Let us remind the reader that a substantial mass growth will be experienced by PBHs with initial masses

$$M_{min} \le M_i < M_{max}. \qquad (27)$$

The lower limit

$$M_{min} = 2 \cdot 10^6 \left(\frac{l}{l_4}\right)^{-1/3} M_4 \qquad (28)$$

follows [3] from the absence of excessive large-angle microwave anisotropy while the upper one

$$M_{max} \simeq \left(\frac{l}{l_4}\right) M_4 \qquad (29)$$

follows from both the condition $r_{BH} = l$ and Eq. (4) at $t = t_c$. Note that BHs with larger masses and radii are the usual 4D BHs which do not experience considerable accretion mass growth [4, 5].

For simplicity we will completely neglect scattering taking $F = 1$ if $r_{BH} < l_{sc}$ and treat the radiation dominated background as a continuous medium taking $F \simeq 1.54$ if $r_{BH} > l_{sc}$. Let us introduce the initial PBH masses M_{i1} and M_{i2} for which the condition $r_{BH} = l_{sc}$ fulfills, respectively, at the final moment $t = t_c$ of the high-energy phase and at the moment $t = t_i$ of the PBH formation. These masses allow us to separate the mass intervals corresponding to different scenarios of PBH mass growth (see Fig. 1), namely, the interval $M_{min} < M_i < M_{i1}$ where $l_{sc} > r_{BH}$ and $F = 1$, the interval $M_{i2} < M_i < M_{max}$ where $l_{sc} < r_{BH}$ and $F \simeq 1.54$ and the mixed interval $M_{i1} < M_i < M_{i2}$ for which a moment $t_i < t_* < t_c$ exists at which $r_{BH}(t_*) = l_{sc}(t_*)$ and one, correspondingly, has $r_{BH} < l_{sc}$, $F = 1$ at $t_i < t < t_*$ and $r_{BH} > l_{sc}$, $F \simeq 1.54$ at $t_* < t < t_c$. Equation (6) can now be directly applied to each interval with constant F

giving a composite formula

$$\frac{M(t_c)}{M_i} = \begin{cases} \left(\frac{t_c}{t_i}\right)^{2/\pi}, & M_{min} < M_i < M_{i1}; \\ \left(\frac{t_*}{t_i}\right)^{2/\pi} \left(\frac{t_c}{t_*}\right)^{16/(3\sqrt{3}\pi)}, & M_{i1} < M_i < M_{i2}; \\ \left(\frac{t_c}{t_i}\right)^{16/(3\sqrt{3}\pi)}, & M_{i2} < M_i < M_{max} \end{cases} \qquad (30)$$

for the coefficient of accretion mass growth during the high-energy phase. The solid lines on Fig. 1 show the coefficient of accretion mass growth as a function of M_i for curvature radii $l/l_4 = 10^{21}, 10^{26}$, and 10^{31} and $f = 0.1$. Long dashed and short dashed lines correspond, respectively, to the values $F = 1$ and $F = 0.5$ used in [6, 7, 8]. From Fig. 1 one can see that Eq. (30) predicts considerably larger mass growth than Eq. (6) with $F = 1$ and 0.5. One can also see that the region $M_{i2} < M_i < M_{max}$ in which Eq. (30) reduces to Eq. (6) with (26) is quite wide.
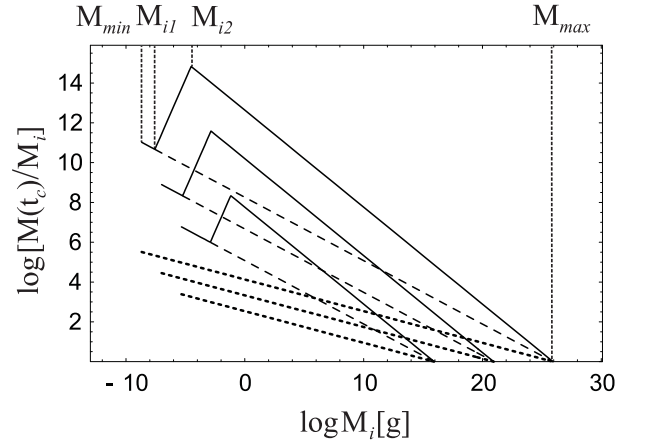

FIG. 1: Accretion mass growth coefficient vs the initial PBH mass for choices $l/l_4 = 10^{21}, 10^{26}$ and 10^{31} (from bottom to top). Solid lines correspond to the PBH mass growth coefficient (30), while long dashed and short dashed ones are obtained from Eq. (6) with fixed accretion efficiencies $F = 1$ and $F = 0.5$, respectively.

Let us keep in mind that the curvature radius is experimentally bound from above by the value $0.2mm \sim 10^{31}l_4$ [13], while its lower limit is determined by the choice of 5D BH evaporation time [3, 4, 5, 6, 7, 8]

$$\frac{t_{evap}}{t_4} \simeq \tilde{g}^{-1} \frac{l}{l_4} \left(\frac{M(t_c)}{M_4}\right)^2, \qquad (31)$$

where $\tilde{g} = 0.023$. Since the most direct ways of PBH search are connected with PBHs completing their evaporation now or at a future time, we limit l by $l_{min} = 10^{20}l_4$ [3] which follows from (31) at $t_{evap} = t_0 = 13.7Gyr$ and $M(t_c) = M_{max}$. Note that at $l/l_4 < 10^{20}$, one will not see any difference from the 4D case.

The accretion efficiency (26) allows us to tighten the constraints imposed on the initial PBH mass fraction [6,

7, 8]

$$\alpha_i = \alpha_i(M_i) = \frac{\rho_{PBH,M_i}(t_i)}{\rho_{rad}(t_i)}, \quad (32)$$

where $\rho_{PBH,M_i}(t_i)$ is the mass density of PBHs with formation mass on the order of M_i and $\rho_{rad}(t_i)$ is the radiation energy density at the moment t_i of such PBH formation. The mass M_i should be evaluated substituting the mass $M(t_c)$ found from Eq. (31) at given l and $t_{evap} = t_0$ into Eq. (30). The PBH mass fraction grows with time starting from the initial value (32) proportionally to $a(t)M(t)$ at $t_i < t < t_c$ and proportionally to $a(t)$ at $t_c < t < t_0$ [6]. Describing the PBH mass growth by Eq. (30) and restricting the present PBH mass density, by 30% of the critical density one obtains new constraints on α_i presented by the solid line in Fig. 2. The latter are much tighter than both the 4D constraint $\alpha_i < f^{-1/2}10^{-18}$ and the old 5D constraints [6] illustrated by long dashed and short dashed lines evaluated using Eq. (6) with $F = 1$ and $F = 0.5$, respectively. The dotted lines both in Fig. 2 and in Figs. 3, 4 below are evaluated using the third line of Eq. (30) in order to illustrate the degree of violation of hydrodynamic approximation in the region $l/l_4 \geq 10^{30}$ where the accretion actually begins in a collisionless regime and only later switches over into a hydrodynamical one being, thus, adequately described by the second line of Eq. (30).
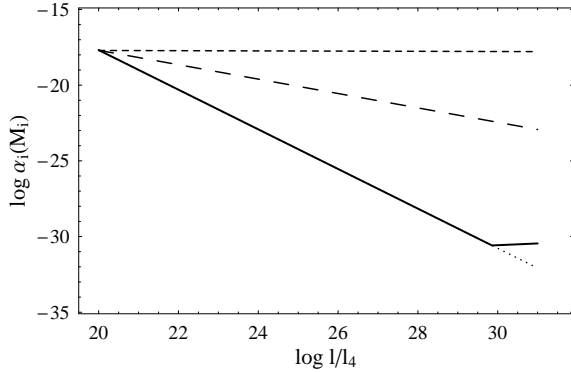

FIG. 2: Constraints on initial PBH mass fraction imposed by the total matter density. Dotted, long dashed and short dashed lines are obtained using PBH mass growth coefficient (6) with $F = 1.54, 1$ and 0.5, respectively.

Equation (30) also allows to revise the constraints following from the measured high-energy diffuse photon spectrum [7] and antiproton excess [8]. Fortunately, it is sufficient to consider the PBHs intensively evaporating at present in both cases [7, 8]. The mass $M^*(l) = M(t_c) \propto l^{-1/2}$ and Hawking temperature $T^*_{BH} = 1/2\pi r_{BH} \propto \sqrt{M^*(l)l} \propto l^{-1/4}$ of such PBHs can be found substituting $t_{evap} = t_0$ into Eq. (31) and then $M^*(l)$ from Eq. (31) into Eq. (2). The Hawking temperature determines the photon energy $E \sim bT^*_{BH}$ with $b \simeq 5$ [6] increasing proportionally to $l^{-1/4}$ from 250 keV to 150 MeV with

the curvature radius variation from $l/l_4 = 10^{31}$ to 10^{20} [3]. The diffuse photon spectrum can be estimated [6, 7] by the formula

$$I(E) = \frac{c}{4\pi}\frac{M^*}{E}n(t_0, M_i(M^*)) \quad (33)$$

where c is the speed of light and

$$n(t_0, M_i(M^*)) =$$
$$\frac{3\alpha_i(M_i)}{2^{17/4}\pi l_4^{9/4}}\frac{a^3(t_{eq})}{a^3(t_0)}f^{1/8}l^{-3/8}t_{eq}^{-3/2}M_i^{-9/8}(M^*) \quad (34)$$

is the present number density of PBHs with mass of the order M^*, where $t_{eq} = 72.6kyr$ [7, 8] is the time of matter-radiation equality and the mass M_i should be found by substituting $M(t_c) = M^*$ into Eq. (30). In particular, one can find that initial masses of PBHs completing their evaporation at present are equal to $M_i = 10^{-4}$ and 10^3g for $l/l_4 = 10^{31}$ and 10^{20}, respectively. Comparing (33) with the observational data collected in [7], one obtains new constraints presented in Fig. 3 by a solid line. These constraints are much tighter than both the 4D constraint $\alpha_i < 10^{-27}$ and the old 5D ones, presented by dashed lines.
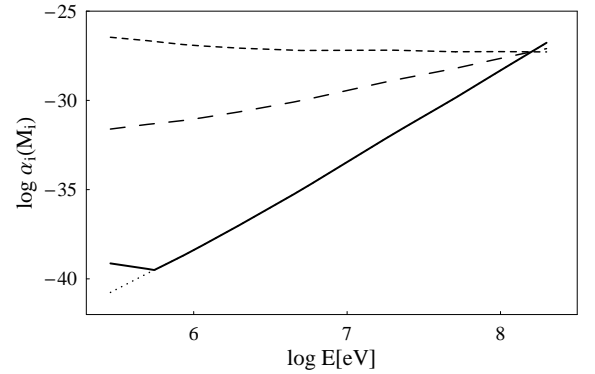

FIG. 3: Constraints on initial PBH mass fraction imposed by the high-energy diffuse photon background. Dotted, long dashed and short dashed lines are obtained using Eq. (6) with $F = 1.54, 1$ and 0.5, respectively.

The antiproton flux from brane PBHs can be schematically written in the form

$$\Phi_{\bar{p}} \propto \frac{dM_i}{dM^*}\frac{M_{GeV}^2}{M_iM^*}Gn(t_0, M_i(M^*)), \quad (35)$$

where $M_{GeV} = M_{GeV}(l)$ is the mass of a PBH with Hawking temperature $T_{BH} \sim 1GeV$ and the factor $G \sim 10^5$ represents the galactic matter density enhancement at the solar neighborhood. Equation (35) differs from equations of ref. [8], combined together in a similar way, solely by the relation (30) of $M^* = M(t_c)$ with M_i. This "small" difference, however, allows us to considerably restrict the "most important result" of Ref. [8] concerning the $\bar{p}$ flux dependence on l. Indeed, using the

PBH mass growth coefficient (6), one obtains [8] from (35) that $\Phi_{\bar{p}} \propto l^p$ with exponent

$$p = \frac{40F - 13\pi}{16(\pi - F)}. \tag{36}$$

Since $p < 0$ at $F \leq 1$ it was argued in [8] that the $\bar{p}$ flux is a *decreasing* function of l (see both dashed lines in Fig. 4) and should be used to set a lower bound on l. However the new value $F \simeq 1.54$ leads to the positive exponent $p \simeq 0.81$ corresponding to *increasing* $\bar{p}$ flux (35) and decreasing constraints on $G\alpha_i$ (solid line in Fig. 4) up to $l/l_4 \simeq 10^{30}$, where the hydrodynamic approximation is violated. These constraints are again much tighter than both the 4D constraint $\alpha_i < 10^{-27}$ and the old 5D ones, presented by dashed lines.
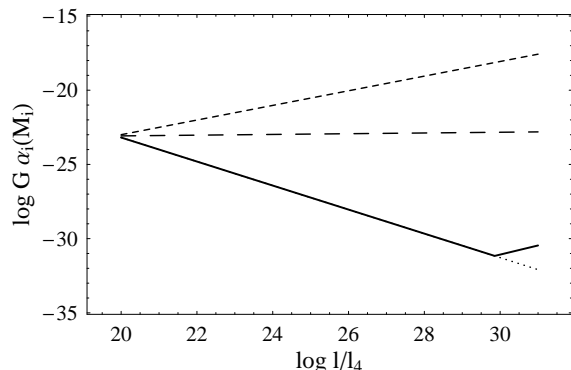

FIG. 4: Constraints on initial PBH mass fraction imposed by the antiproton excess. Dotted, long dashed and short dashed lines are obtained using Eq. (6) with $F = 1.54, 1$ and 0.5, respectively.

Because of violation of hydrodynamic approximation at $l/l_4 > 10^{30}$ and in the corresponding photon energy region $E \leq 500 keV$ all the considered constraints reach their maxima at $l/l_4 \simeq 10^{30}$. Figures 2-4 demonstrate that the tightest constraints following from the critical density limit and measurements of the high-energy diffuse photon background and antiproton excess at $l/l_0 \simeq 10^{30}$ amount, respectively, to $\alpha_i \simeq 10^{-31}, 10^{-39}$ and 10^{-36}. Since the tightness of all the constraints increases with the curvature radius l, all of them can be used to set an upper bound on l at $l/l_4 \leq 10^{30}$.

To summarize, particle collisions make hydrodynamic approximation adequate to describe the accretion of the radiation dominated background onto PBHs during most of the high-energy phase of the RS2 braneworld scenario. Continuous background is characterized by 54% higher accretion efficiency onto PBHs than that of collisionless relativistic particles. This higher accretion efficiency provides larger PBH mass growth during the high-energy phase and makes it possible to obtain much tighter constraints on initial mass fraction than those found in [6, 7, 8] as well as than the constraint equal to 10^{-27} obtained in the standard 4D cosmology. The tightness of the obtained constraints mostly increases with curvature radius allowing to restrict it from above.

[1] Ya. B. Zel'dovich, I. D. Novikov, *Astron. Zh. (USSR)* **43**, 758 (1966) [Sov. Astron. **10**, 602 (1967)].
[2] S.W. Hawking, Mon. Not. R. Astron. Soc. **152**, 75 (1971).
[3] R. Guedens, D. Clancy and A. R. Liddle, *Phys. Rev. D* **66**, 043513 (2002).
[4] A. S. Majumdar, *Phys. Rev. Lett.* **90**, 031303 (2003).
[5] R. Guedens, D. Clancy and A. R. Liddle, *Phys. Rev. D* **66**, 083509 (2002).
[6] D. Clancy, R. Guedens and A. R. Liddle, *Phys. Rev. D* **68**, 023507 (2003).
[7] Y. Sendouda, S. Nagataki and K. Sato, *Phys. Rev. D* **68**, 103510 (2003).
[8] Y. Sendouda, K. Kohri, S. Nagataki and K. Sato, *Phys. Rev. D* **71**, 063512 (2005).

[9] S. Shapiro and S. Teukolsky, *Black Holes, White Dwarfs and Neutron Stars* (Wiley, New York, 1983).
[10] Ya. B. Zel'dovich, I. D. Novikov, *Relativistic Astrophysics, Vol.I: Stars and Relativity* (University of Chicago Press, Chicago, 1971).
[11] H. Bondi, *Mon. Not. Roy. Astron. Soc.* **112**, 195 (1952).
[12] F.C. Michel, *Astrophys. Space Sci.*, **15**, 153, (1972).
[13] J.C. Long et al. *Nature* (London) **421**, 922 (2003).
[14] L.D. Landau and E.M. Lifshitz, *Fluid Dynamics* (Pergamon Press, Oxford, 1987), 2nd ed.
[15] H.V. Klapdor-Kleingrothaus and K. Zuber, *Teilchenastrophysik* (B.G. Teubner GmbH, Stuttgart, 1997).